

Reconstruction of Photon Conversions in the MPD Experiment

Evgeny Kryshen ^{1,*},[†] , Dmitry Ivanishchev ¹, Dmitry Kotov ^{1,2}, Mikhail Malaev ¹, Victor Riabov ^{1,3} and Yuriy Ryabov ¹

¹ Petersburg Nuclear Physics Institute Named by B. P. Konstantinov of NRC “Kurchatov Institute”, 1 mkr. Orlova roshcha, 188300 Gatchina, Russia; ivanishchev_da@pnpi.nrcki.ru (D.I.); kotov_do@pnpi.nrcki.ru (D.K.); Mikhail.Malaev@cern.ch (M.M.); riabov_vg@pnpi.nrcki.ru (V.R.); ryabov_yg@pnpi.nrcki.ru (Y.R.)

² Peter the Great St. Petersburg Polytechnic University, Polytechnicheskaya 29, 195251 St. Petersburg, Russia

³ MEPhI (Moscow Engineering Physics Institute), National Research Nuclear University, 31 Kashirskoe Shosse, 115409 Moscow, Russia

* Correspondence: kryshen_el@pnpi.nrcki.ru

† For the MPD Collaboration.

Abstract: Spectra of thermal photons carry important information on the temperature of the hot and dense medium produced in heavy ion collisions. Photons can be measured via their conversion into electron-positron pairs in the detector material. In this contribution, challenges in the photon reconstruction are discussed and feasibility studies on photon conversion measurements in the future multipurpose detector (MPD) experiment at NICA are presented. The obtained results indicate good prospects for thermal photon measurements.

Keywords: photon conversions; thermal photons; MPD experiment; NICA



Citation: Kryshen, E.; Ivanishchev, D.; Kotov, D.; Malaev, M.; Riabov, V.; Ryabov, Y. Reconstruction of Photon Conversions in the MPD Experiment. *Particles* **2021**, *4*, 55–62. <https://doi.org/10.3390/particles4010008>

Academic Editor: Peter Senger

Received: 13 January 2021

Accepted: 7 February 2021

Published: 17 February 2021

Publisher’s Note: MDPI stays neutral with regard to jurisdictional claims in published maps and institutional affiliations.



Copyright: © 2021 by the authors. Licensee MDPI, Basel, Switzerland. This article is an open access article distributed under the terms and conditions of the Creative Commons Attribution (CC BY) license (<https://creativecommons.org/licenses/by/4.0/>).

1. Introduction

The future multipurpose detector (MPD) at the Nuclotron-based Ion Collider Facility (NICA) is aimed towards the studies of hot and dense medium produced in heavy ion collisions in the range of center-of-mass energies $\sqrt{s_{NN}} = 4$ to 11 GeV [1]. In contrast to heavy ion collisions at the Relativistic Heavy Ion Collider (RHIC) and the Large Hadron Collider (LHC) corresponding to vanishing net baryonic densities, the matter produced in the NICA energy range is expected to reach large baryonic densities far exceeding the normal nuclear density ρ_0 . According to several model calculations described in [2], the nuclear fireball created in central heavy ion collisions will be compressed to a density above $8\rho_0$ already at the lowest NICA energy of $\sqrt{s_{NN}} = 4$ GeV. At higher NICA energies, the maximum net baryon density is expected to increase further. Thus, heavy ion collisions at NICA complement experimental efforts at RHIC and LHC colliders in the studies of the phase diagram of nuclear matter and searches for the deconfinement phase transition. This energy range will be also studied by the STAR experiment in the RHIC beam energy scan II program (down to $\sqrt{s_{NN}} = 7.7$ GeV in the collider mode and down to $\sqrt{s_{NN}} = 3$ GeV in the fixed target mode) [3]. Even lower center-of-mass energies ($\sqrt{s_{NN}}$ from 2 to 5 GeV) will be accessed by the High Acceptance DiElectron Spectrometer (HADES) and the Compressed Baryonic Matter (CBM) experiments at the Facility for Antiproton and Ion Research (FAIR) [4,5]. This broad and complementary research program provides an opportunity to probe the nuclear equation-of-state at high baryonic densities which is necessary for an understanding of neutron star interiors [6].

The construction of the MPD experiment will be carried out in two stages. In the first stage, the time projection chamber (TPC), the time-of-flight (TOF) detector, the electromagnetic calorimeter (EMCal), the forward hadron calorimeter (FHCAL), and the fast forward detector (FFD) will be installed. The TPC will be placed in a superconducting solenoid providing efficient tracking, particle identification (PID) and momentum measurements

in a wide pseudorapidity range $|\eta| < 1.2$. The TOF detector will be based on multigap resistive plate counters and will be used to perform particle identification up to a momenta of about 2 GeV/c. The ECal will be used to identify electrons, photons, and neutral hadrons in the central rapidity region while FHCAL is aimed for centrality determination purposes. The FFD will be used for trigger purposes. In the second stage, the inner tracking system (ITS) located between the beam pipe and the TPC will be installed for a precise reconstruction of primary and secondary vertices.

Among various observables studied in heavy ion collisions, direct photons play a special role. They are emitted at all stages of the evolution of the produced hadronic matter and carry information on the temperature of the medium at a time of their emission [7]. One usually distinguishes high-energy prompt photons produced in hard scatterings at early stages and low-energy thermal photons radiated by the expanding fireball. The inverse slope of the thermal photon momentum distribution reflects the effective temperature averaged over space-time evolution of the medium. The effective photon temperatures measured at RHIC [8] and LHC energies [9] appear to be much larger than the temperature of about 170 MeV predicted for the transition from the hadron gas to the deconfined quark-gluon plasma phase [10]. According to the RHIC beam energy scan results [11], the effective temperature tends to decrease towards lower collision energies. However, according to theoretical predictions [12,13], the initial temperatures in central Au-Au collisions at NICA energies still raise above 200 MeV, while time-averaged effective temperatures are expected to be in the range from 150 to 170 MeV. Thus the MPD experiment has a unique opportunity to perform precision direct photon measurements and trace the transition from hadronic to partonic degrees of freedom in the NICA energy range.

One of the challenges in the direct photon measurements is related to the fact that the measured photon spectra are dominated by decay photons originating mainly from neutral π and η meson decays. In order to get the direct photon spectrum, the decay contribution has to be subtracted from the inclusive photon spectrum. Usually one constructs a ratio R_γ of inclusive and decay photon yields where decay photon yields are determined from the measured spectra of π^0 and η mesons [7].

The MPD experiment will explore two methods to measure photons. The first method will utilize the ECal capabilities. The second method will be based on the reconstruction of photons converted in the detector material into electron-positron pairs measured in the TPC. The latter method has an advantage of much better energy resolution at low energies and smaller combinatorial backgrounds in neutral meson measurements. However the conversion method has a disadvantage of a much smaller efficiency that is proportional to the effective radiation length of the detector material in front of the tracking volume. In the first stage of the MPD experiment, photons will mainly be converted in the beam pipe (0.3% X_0) and in the inner TPC vessel structures (2.4% X_0) therefore the conversion reconstruction efficiency will hardly exceed a few percent.

In this contribution, feasibility studies on photon conversion measurements in the future MPD experiment at NICA are presented.

2. Photon Reconstruction

The studies of the photon conversion probability were performed with the GEANT4 package coupled to the official MpdRoot framework used for Monte Carlo simulations of the MPD detector response, track reconstruction, and pattern recognition. The photon conversion probability is shown in Figure 1 as a function of the photon transverse momentum p_T for photons in the central pseudorapidity range $|\eta| < 1$. The conversion probability rapidly grows towards a higher momenta and reaches a plateau of about 3.5% at $p_T > 0.5$ GeV/c. As shown in Figure 1, an application of fiducial selection criteria on the transverse momentum ($p_T^e > 50$ MeV/c) and pseudorapidity ($|\eta_e| < 1$) of conversion electrons and positrons results in a reduction of the fraction of accepted photons, mainly at a low transverse momenta.

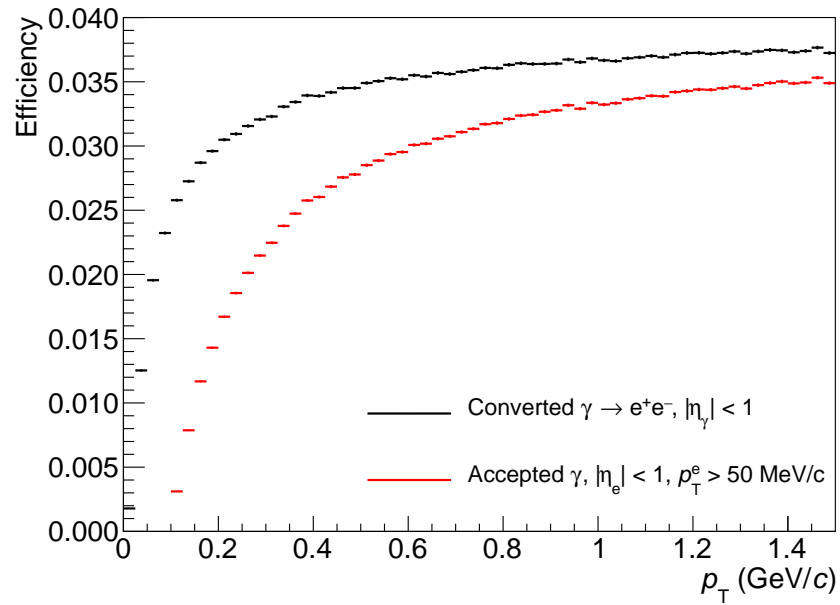


Figure 1. Photon conversion probability (black) and acceptance (red) as a function of the photon transverse momentum.

Reconstruction of converted photons requires the efficient identification of electrons. The MPD experiment provides efficient electron separation using energy loss measurements in the TPC in the momentum range $0.2 < p_e < 0.5 \text{ GeV}/c$ while TOF measurements allow one to access the momentum region $p_e < 0.3 \text{ GeV}/c$. A dedicated procedure to select electron candidates has been developed. Tracks with energy loss and effective squared mass measurements are selected in ± 4 standard deviations around their mean values at a given momentum. Distributions of energy losses in the TPC and reconstructed squared mass in the TOF for electrons are shown in Figure 2 together with corresponding selection limits.

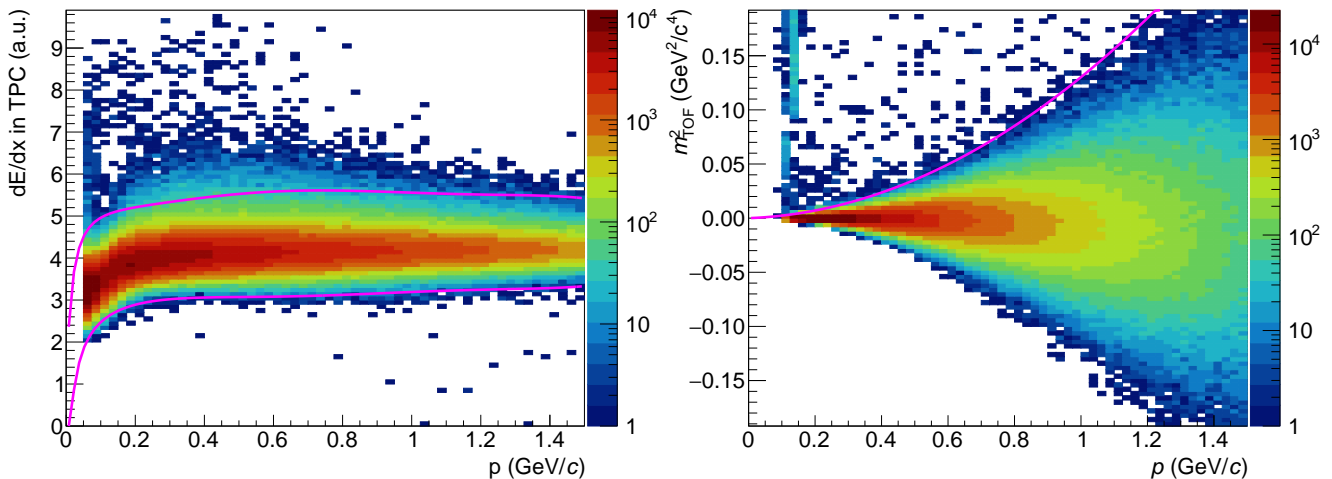


Figure 2. (Left) Distribution of energy losses in the time projection chamber (TPC) for electrons as a function of momentum. (Right) Distribution of reconstructed squared mass in the time-of-flight (TOF) for electrons as a function of momentum. Selection limits are shown with magenta lines.

Secondary vertices of electron-positron pairs from conversions were reconstructed using a dedicated MpdParticle tool that allows one to build a vertex and determine its parameters for any combination of positive and negative tracks. The tool is based on the Kalman filter algorithm [14]. Figure 3 shows typical distributions of the χ^2 parameter representing the quality of secondary vertices for signal electron-positron pairs and random

background pairs as a function of pair p_T . A requirement $\chi^2 < 10$, used to reject random pairs of tracks, is also shown in the figure.

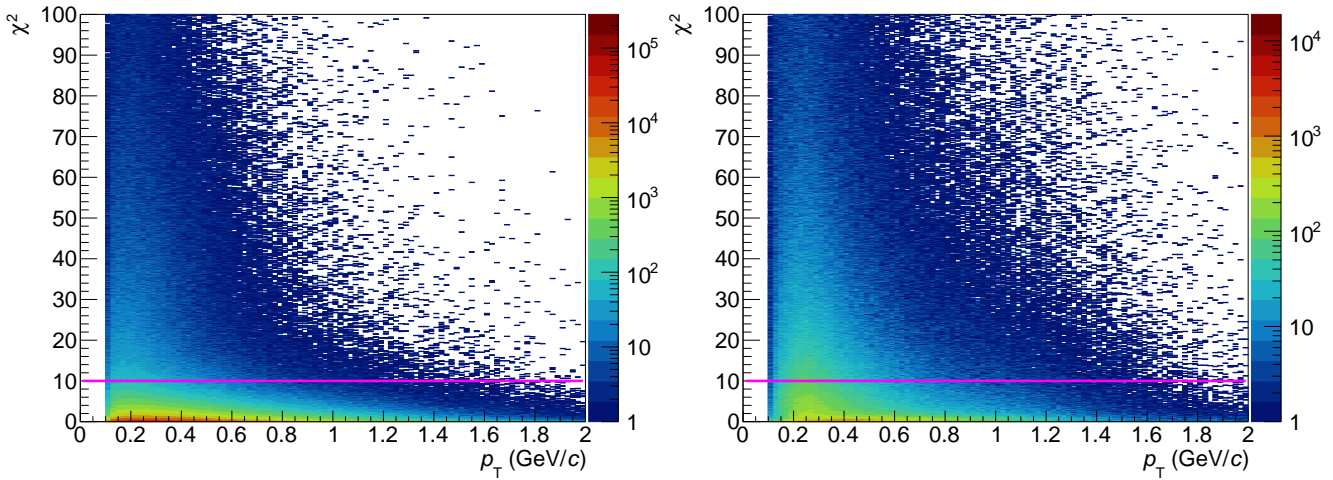


Figure 3. Distributions of signal (left) and background (right) pairs as a function of the vertex χ^2 and transverse momentum of the reconstructed pair. Selection limits are shown with magenta lines.

The χ^2 selection does not remove background pairs of tracks coming from the primary vertex, such as electron-positron pairs from Dalitz decays, since they are characterized by small distances of the closest approach. In order to remove these pairs from the sample of conversion candidates, one can reject secondary vertices at small distances from the primary vertex. Distributions of signal and background pairs are shown in Figure 4 as a function of the radial position of the vertex (R_{vtx}) and transverse momentum of the reconstructed pair. Signal conversion pairs originate from radii close to the beam pipe and inner TPC structures while random background pairs mainly come from radii below 20 cm. The radial resolution of secondary vertices is rather poor therefore a tight requirement on $R_{vtx} > 10$ cm is used to suppress the background from random pairs of primary tracks.

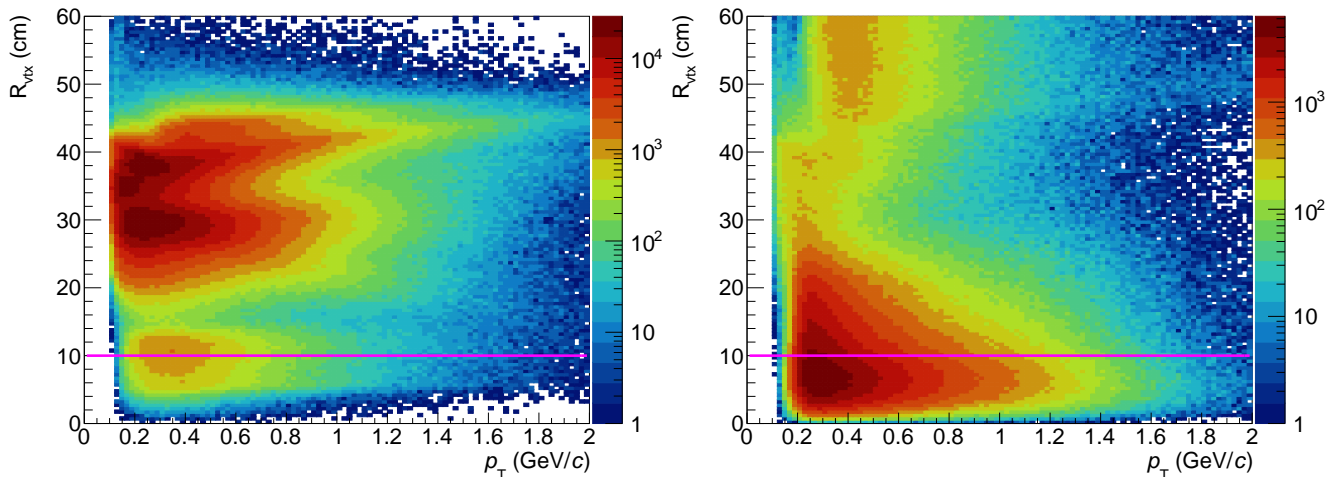


Figure 4. Distributions of signal (left) and background (right) pairs as a function of radial position of the vertex and transverse momentum of the reconstructed pair. Selection limits are shown with magenta lines.

Background pairs of tracks can be further suppressed using the selection on the invariant mass of the pair assuming electron mass hypothesis for daughter tracks. Distributions of signal and background pairs as a function of invariant mass and transverse momentum of the reconstructed pair are shown in Figure 5. The invariant masses for conversion pairs are close to zero. As for the background pairs, the distribution is much broader though the ridge at small masses is also visible. The ridge corresponds to electron-positron pairs

coming from a primary vertex (e.g., from Dalitz decays) and can be suppressed with R_{vtx} selection. Since the invariant mass resolution depends on daughter track momenta, we use a p_T -dependent selection: $m_{\text{pair}} < 0.0226 + 0.0174 p_T^{\text{pair}}$ where m_{pair} and p_T^{pair} are measured in GeV units.

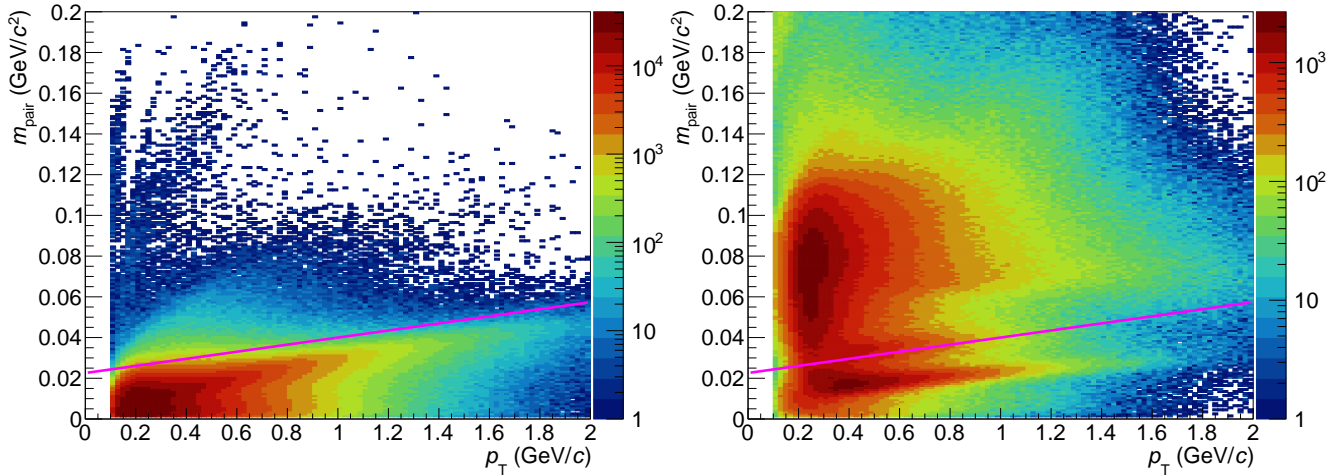


Figure 5. Distributions of signal (left) and background (right) pairs as a function of invariant mass and transverse momentum of the reconstructed pair. Selection limits are shown with magenta lines.

The reconstructed total momentum of electron-positron pairs from converted direct photons should point to the primary vertex. The selection on the pointing angle, i.e., the angle between pair momentum vector and direction to the primary vertex, can be used to suppress the background further. Distributions of signal and background pairs as a function of pointing angle and transverse momentum of the reconstructed pair are shown in Figure 6. The pointing angle resolution improves towards higher transverse momentum of the pair. Therefore the following p_T^{pair} -dependent selection on the pointing angle was found to be optimal: $\theta < \exp(-2.777 - 2.798 p_T^{\text{pair}}) + 0.0175$ where p_T^{pair} is measured in GeV units.

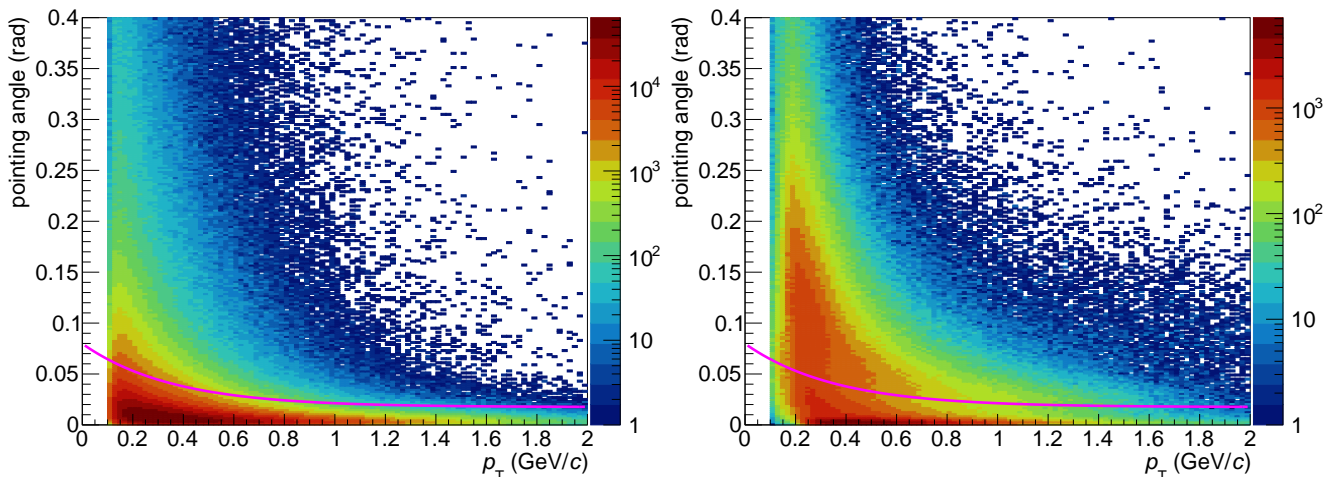


Figure 6. Distributions of signal (left) and background (right) events as a function of the pointing angle and transverse momentum of the photon pair. Selection limits are shown with magenta lines.

Finally the important difference between track pairs from photon conversions and weak decays is that the opening angle between electron and positron tracks from conversions is small resulting in a preferred direction of the dielectron plane with respect to the magnetic field vector. Distributions of the angle Ψ_{pair} between the plane perpendicular to the magnetic field and the plane which is spanned by the e^+ and e^- momentum vectors

is shown in Figure 7 for signal and background pairs. A selection $|\Psi_{\text{pair}}| < 0.1$ helps to improve the purity of the converted photon sample.

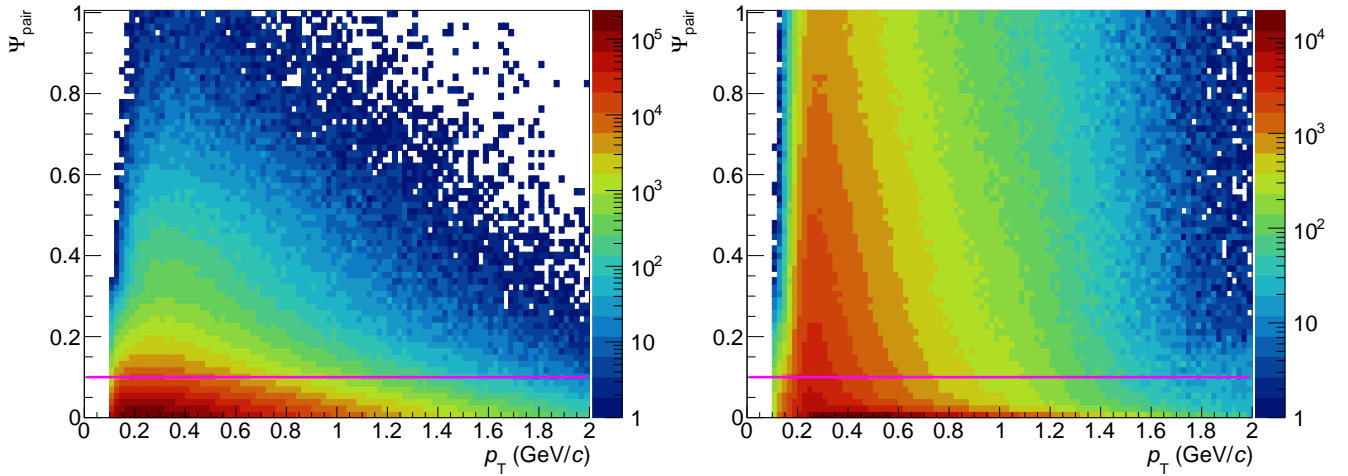


Figure 7. Distributions of signal (left) and background (right) pairs as a function of the Ψ_{pair} angle and transverse momentum of the reconstructed pair. Selection limits are shown with magenta lines.

All the selection criteria were carefully optimized using a multivariate technique with the aim to maximize significance of the signal. The reconstruction efficiency after optimized single electron track cuts and after pair cuts is shown in Figure 8. The conversion reconstruction efficiency reaches a maximum of about 1.5%. Contribution of the non-photon background does not exceed 10–20% and can be further improved with tighter selection criteria.

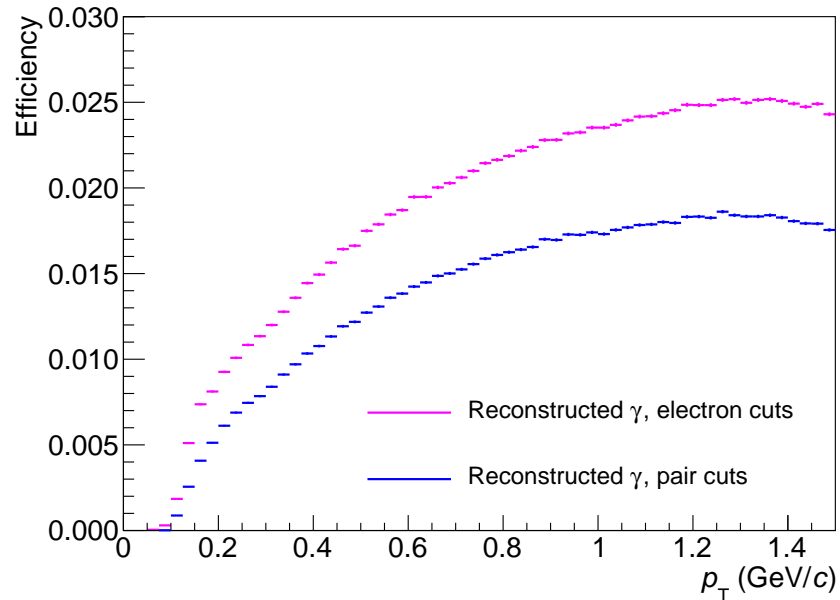


Figure 8. Photon reconstruction efficiency after single electron (magenta) and electron pair (blue) selection criteria.

3. Direct and Decay Photon Production Estimates

Widely used general purpose event generators do not simulate the production of direct photons and hence the direct photon feasibility studies require external inputs. A data-driven method was developed to estimate the spectra of direct photons in Au-Au collisions at NICA energies. The method relies on the universal scaling of direct photon yields with the (pseudo)rapidity density of final state charged particles $dN_{\text{ch}}/d\eta$ observed

at RHIC and LHC energies [11]. The PHENIX experiment found that the integrated yields of direct photons above $p_T > 1$ GeV/c scale as a power law $(dN_{ch}/d\eta)^{1.25}$ in a wide range of centralities and collision energies. This scaling works well for collisions with $dN_{ch}/d\eta > 20$ and is broken only at lower multiplicities. Assuming the scaling still holds at NICA energies for relatively high multiplicities, one can expect its validity for Au-Au collisions in the range of (0–60)% centrality at $\sqrt{s_{NN}} = 11$ GeV and (0–40)% centrality at $\sqrt{s_{NN}} = 4$ GeV.

Transverse momentum spectra of direct photons can be also predicted assuming a universal p_T scaling observed by PHENIX in the region $p_T > 0.4$ GeV/c [11,15]. Differential direct photon yields in Au-Au collisions at $\sqrt{s_{NN}} = 4$ and 11 GeV were calculated in the region of $p_T > 0.6$ GeV/c assuming a $\frac{d^3N}{d^2p_T dy} = 2.755 \times 10^{-4} \cdot p_T^{-4.5} \times (dN_{ch}/d\eta)^{1.25}$ dependence as shown in Figure 9, left. In the region of low $p_T < 0.6$ GeV/c, direct photon spectra were assumed to follow the thermal spectrum $dN/dp_T \sim p_T \exp(-p_T/T_{eff})$ with a conservative effective temperature $T_{eff} = 150$ MeV [12,13].

The decay photon spectrum coming from $\pi^0 \rightarrow \gamma\gamma$ and $\eta \rightarrow \gamma\gamma$ decays was estimated in accordance with projections on p_T -differential π^0 and η meson measurements described in [16–18]. The inclusive photon yields were obtained as a sum of direct and decay photon yields. The excess photon ratio R_γ was calculated as a ratio of an inclusive photon spectrum to decay photon spectrum and is shown in Figure 9, right, in three centrality classes. The performed study shows that R_γ significantly exceeds unity starting from 1.03 for semi-central collisions and increases with p_T exceeding 1.2 at 1.4 GeV similar to previous measurements at higher energies. Assuming a sample of about 10^9 minimum bias events, expected statistical uncertainties on the inclusive photon spectrum will not exceed 1% in the considered p_T range. The precision of the R_γ ratio and the direct photon spectrum measurement will be limited mainly by the systematic uncertainty related to the knowledge of the decay photon contribution in the inclusive photon yield. According to the experience of other experiments, typical systematic uncertainties on R_γ can be reduced to about 2% [11]. Thus the obtained R_γ estimates justify the possibility to measure direct photon production with the MPD detector down to low transverse momenta.

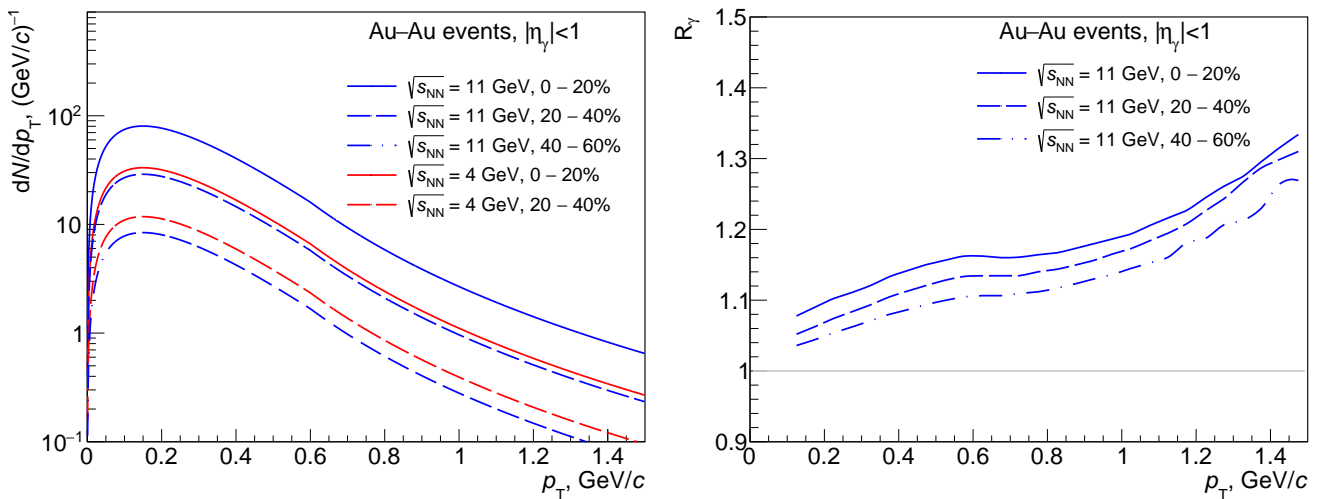


Figure 9. The expected direct photon spectra (left) and excess photon ratio R_γ (right) as a function of the photon transverse momentum in Au-Au collisions at NICA energies.

4. Conclusions

In this contribution, we summarized that photons serve as valuable probes of the hot and dense medium produced in heavy ion collisions. The procedure of photon reconstruction with the photon conversion method was described. The feasibility of measuring thermal photon production spectra in Au-Au collisions at $\sqrt{s_{NN}} = 11$ GeV with the MPD detector at NICA was shown.

Author Contributions: Conceptualization, E.K., V.R., Y.R.; methodology, E.K. and V.R.; software, M.M., Y.R. and D.I.; validation, D.K. and D.I.; formal analysis, E.K.; investigation, E.K. and V.R.; writing—original draft preparation, E.K.; writing—review and editing, V.R.; visualization, E.K.; supervision, D.I. and E.K.; project administration, D.I.; funding acquisition, E.K. All authors have read and agreed to the published version of the manuscript.

Funding: This research was funded by RFBR according to the research project # 18-02-40045 and partially supported by the National Research Nuclear University MEPhI in the framework of the Russian Academic Excellence Project (contract No. 02.a03.21.0005, 27.08.2013).

Conflicts of Interest: The funders had no role in the design of the study; in the collection, analyses, or interpretation of data; in the writing of the manuscript, or in the decision to publish the results.

References

1. Golovatyuk, V.; Kekelidze, V.; Kolesnikov, V.; Rogachevsky, O.; Sorin, A. The Multi-Purpose Detector (MPD) of the collider experiment. *Eur. Phys. J. A* **2016**, *52*, 212. [[CrossRef](#)]
2. Arsene, I.C.; Bravina, L.V.; Cassing, W.; Ivanov, Y.B.; Larionov, A.; Randrup, J.; Russkikh, V.N.; Toneev, V.D.; Zeeb, G.; Zschesche, D. Dynamical phase trajectories for relativistic nuclear collisions. *Phys. Rev. C* **2007**, *75*, 034902. [[CrossRef](#)]
3. Odyniec, G. Beam Energy Scan Program at RHIC (BES I and BES II)—Probing QCD Phase Diagram with Heavy-Ion Collisions. *PoS* **2019**, *CORFU2018*, 151. [[CrossRef](#)]
4. Senger, P. Probing dense QCD matter in the laboratory—The CBM experiment at FAIR. *Phys. Scr.* **2020**, *95*, 074003. [[CrossRef](#)]
5. Salabura, P. Studying Baryonic Matter with HADES at GSI/FAIR. *Acta Phys. Polon. B* **2019**, *50*, 1205–1216. [[CrossRef](#)]
6. Klähn, T.; Blaschke, D.; Typel, S.; Van Dalen, E.N.E.; Faessler, A.; Fuchs, C.; Wolter, H.H. Constraints on the high-density nuclear equation of state from the phenomenology of compact stars and heavy-ion collisions. *Phys. Rev. C* **2006**, *74*, 035802. [[CrossRef](#)]
7. David, G. Direct real photons in relativistic heavy ion collisions. *Rept. Prog. Phys.* **2020**, *83*, 046301. [[CrossRef](#)] [[PubMed](#)]
8. Adare, A.; Afanasiev, S.; Aidala, C.; Ajitanand, N.N.; Akiba, Y.; Al-Bataineh, H.; Alexander, J.; Al-Jamel, A.; Aoki, K.; Aphecetche, L.; et al. Enhanced production of direct photons in Au+Au collisions at $\sqrt{s_{NN}} = 200$ GeV and implications for the initial temperature. *Phys. Rev. Lett.* **2010**, *104*, 132301. [[CrossRef](#)] [[PubMed](#)]
9. Adam, J.; Adamova, D.; Aggarwal, M.M.; Rinella, G.A.; Agnello, M.; Agrawal, N.; Ahammed, Z.; Ahn, S.U.; Aiola, S.; Akindinov, A.; et al. Direct photon production in Pb-Pb collisions at $\sqrt{s_{NN}} = 2.76$ TeV. *Phys. Lett. B* **2016**, *754*, 235–248. [[CrossRef](#)]
10. Laermann, E.; Philipsen, O. The Status of lattice QCD at finite temperature. *Ann. Rev. Nucl. Part. Sci.* **2003**, *53*, 163–198. [[CrossRef](#)]
11. Adare, A.; Afanasiev, S.; Aidala, C.; Ajitan, N.N.; Akiba, Y.; Akimoto, R.; Fleuret, F. Beam Energy and Centrality Dependence of Direct-Photon Emission from Ultrarelativistic Heavy-Ion Collisions. *Phys. Rev. Lett.* **2019**, *123*, 022301. [[CrossRef](#)] [[PubMed](#)]
12. Endres, S.; van Hees, H.; Bleicher, M. Photon and dilepton production at the Facility for Antiproton and Ion Research and beam-energy scan at the Relativistic Heavy-Ion Collider using coarse-grained microscopic transport simulations. *Phys. Rev. C* **2016**, *93*, 054901. [[CrossRef](#)]
13. Rapp, R.; van Hees, H. Thermal Dileptons as Fireball Thermometer and Chronometer. *Phys. Lett. B* **2016**, *753*, 586–590. [[CrossRef](#)]
14. Luchsinger, R.; Grab, C. Vertex reconstruction by means of the method of Kalman filter. *Comput. Phys. Commun.* **1993**, *76*, 263–280. [[CrossRef](#)]
15. Khachatryan, V.; Praszalowicz, M. Scaling properties of direct photon yields in heavy ion collisions. *Eur. Phys. J. C* **2020**, *80*, 670. [[CrossRef](#)]
16. Kryshen, E.; Ivanishchev, D.; Kotov, D.; Malaev, M.; Riabov, V.; Ryabov, Y. Perspectives of thermal photon measurements in heavy ion collisions at NICA. *EPJ Web Conf.* **2019**, *222*, 02006. [[CrossRef](#)]
17. Kryshen, E.; Ivanishchev, D.; Kotov, D.; Malaev, M.; Riabov, V.; Ryabov, Y. Study of neutral meson production with photon conversions in the MPD experiment at NICA. *J. Phys. Conf. Ser.* **2019**, *1400*, 055055. [[CrossRef](#)]
18. Ivanishchev, D.; Kryshen, E.; Kotov, D.; Malaev, M.; Riabov, V.; Ryabov, Y. Feasibility of thermal photon measurements in heavy ion collisions at NICA energies. *J. Phys. Conf. Ser.* **2020**, *1690*, 012109. [[CrossRef](#)]